PERGAMON

International Journal of Heat and Mass Transfer 43 (2000) 4229–4248

International Journal of HEAT and MASS TRANSFER

www.elsevier.com/locate/ijhmt

A numerical study on three-dimensional conjugate heat transfer of natural convection and conduction in a differentially heated cubic enclosure with a heat-generating cubic conducting body

Man Yeong Ha*, Mi Jung Jung

School of Mechanical Engineering, Pusan National University, San 30, Jangjeon-Dong, Kumjung-Ku, Pusan 609-735, South Korea

Received 24 September 1999; received in revised form 10 February 2000

Abstract

A comprehensive numerical study has been conducted to investigate three-dimensional, steady, conjugate heat transfer of natural convection and conduction in a vertical cubic enclosure within which a centered, cubic, heat-conducting body generates heat. The physical model considered here assumes that a temperature difference exists across the enclosure (right cold wall and left hot wall) and the body generates a constant amount of heat. Under these conditions, the flow inside the enclosure is driven by two temperature differences: a temperature difference across the enclosure and a temperature difference caused by the heat source. A ratio of these two temperatures is a key parameter in this study. The steady, three-dimensional governing equations are written in a dimensionless form with dimensionless parameters that decide the heat transfer and flow characteristics in this system. The analysis is conducted by observing variations of the velocity vectors, pathlines, and isotherms for different Rayleigh numbers and temperature-difference ratios. The details of the three-dimensional flow and isotherms are described in order to investigate the effects of three-dimensionalities on the fluid flow and thermal characteristics in the enclosure. The variations of Nusselt numbers on the hot and cold walls are also presented to show the overall heat transfer characteristics inside the enclosure. © 2000 Elsevier Science Ltd. All rights reserved.

1. Introduction

An important class of natural convection heat transfer is that related to buoyancy-driven flows moving within an enclosure. The heat transfer and flow characteristics of natural convection in rectangular enclosures have attracted much research, due to their many practical engineering applications, such as in building insulation, solar energy collection, cooling of heat-generating components in the electrical and nuclear industries, and flows in rooms due to thermal energy sources[1–3]. There are two elementary classes of natural convection flows in enclosures. The first is a horizontal cavity with heating from below and with adiabatic vertical walls. Natural convection flows in a horizontal cavity are characteristics of Rayleigh–Benard convection and of practical problems of electronic equipment

* Corrensponding author. Tel.: +82-51-510-2440; fax: +82-51-512-9835.

E-mail address: myha@hyowon.pusan.ac.kr (M.Y. Ha).

0017-9310/00/$ - see front matter © 2000 Elsevier Science Ltd. All rights reserved.
PII: S0017-9310(00)00063-6

Nomenclature

A^*	area ratio ($=W^2/L^2$)
C_p	constant pressure specific heat
g	gravitational acceleration
k_f	thermal conductivity of fluid
k_s	thermal conductivity of solid
k^*	thermal conductivity ratio ($=k_s/k_f$)
L	length of the enclosure
Nu	local Nusselt number
$\overline{Nu}$	average Nusselt number
$\tilde{P}$	dimensionless pressure
Pr	Prandtl number ($=\nu/\alpha$)
$\dot{q}$	heat generation per unit volume
Ra	Rayleigh number ($=g\beta(T_h-T_c)L^3/\nu\alpha$)
T	temperature
T_c	cold wall temperature
T_h	hot wall temperature
u	velocity in the horizontal direction
$\tilde{u}$	dimensionless velocity in the horizontal direction
v	velocity in the vertical direction
$\tilde{v}$	dimensionless velocity in the vertical direction
w	velocity in the transverse direction
$\tilde{w}$	dimensionless velocity in the transverse direction
W	length of the conducting body
x	dimensionless horizontal coordinate
x^*	horizontal coordinate
y	dimensionless vertical coordinate
y^*	vertical coordinate
z	dimensionless transverse coordinate
z^*	transverse coordinate
α	thermal diffusivity
β	thermal expansion coefficient
ΔT^*	temperature-difference ratio ($=(qW^2/k_f)/(T_h-T_c)$)
θ	dimensionless temperature
ν	kinematic viscosity
ρ	density

Subscripts

c	cold
f	fluid
h	hot
max	maximum
min	minimum
s	solid

cooling, heat exchanger design, meteorology of the earth's atmospheric boundary layers, etc. The second is a vertical cavity with two vertical walls at different temperatures and with adiabatic horizontal surfaces. Natural convection flows in a vertical cavity are probably the most considered configuration in the studies of natural convection because of their relative simplicity and practical importance. Two- and three-dimensional numerical analyses for a vertical cavity have been performed in the past over a wide range of Rayleigh numbers [4–10]. These studies suggested a set of benchmark numerical results for the two- and three-dimensional, steady, laminar and turbulent flows for different Rayleigh numbers, and they also compared their computational results with the experimental ones [11–13].

Considerable research has also been performed with various obstacles in the form of partitions or partial baffles placed inside enclosures [14]. Studies revealed that these kinds of obstructions could change the characteristics of the flow and heat transfer in an enclosure. Moreover, the effects of a centered, squared, heat-conducting body with and without heat generation on natural convection in a vertical square enclosure have been investigated by several researchers [15,16]. Natural convection in a vertical cavity with a centered, squared, heat-conducting body is a conjugate heat transfer problem of natural convection and conduction heat transfer, and becomes more complex compared to that without a conduction body. House et al. [14] numerically examined natural convection in a vertical square enclosure with a centered, squared, heat-conducting body without heat generation. They found that heat transfer across the enclosure may be enhanced or decreased by a body with a thermal conductivity ratio of less than or greater than unity. Oh et al. [15] and Ha et al. [16] investigated both the steady and the unsteady natural convection processes when a temperature difference exists across an enclosure and, at the same time, when a conducting body generates heat within the enclosure. Under these conditions, the flow inside the enclosure is driven by two temperature differences: a temperature difference across the enclosure and a temperature difference caused by the heat source. A ratio of these two temperature differences is a very important factor in deciding the heat transfer and flow characteristics of the enclosure. These studies investigated the effects of the Rayleigh numbers, the Prandtl numbers, the thermal conductivity ratio, the heat capacity ratio, and the temperature-difference ratio on variations of streamlines, isotherms, heat-

lines, and the average Nusselt numbers on hot and cold walls.

Most of the previous studies on natural convection in a vertical cavity with a centered, squared, heat-conducting body with and without heat generation have been two-dimensional [14–16]. There has been little study on the three-dimensional natural convection process in a vertical cavity when a temperature difference exists across an enclosure and, at the same time, when a conducting body generates heat within the enclosure. Three-dimensional calculations are highly desirable because the real flow in a vertical cavity is three-dimensional. In the present study, we investigate three-dimensional heat transfer and flow phenomena of natural convection in a vertical cubic enclosure within which a centered, cubic, heat-conducting body generates heat. We investigate the flow and heat transfer characteristics of a system by observing variations in pathlines and isotherms for different Rayleigh numbers and temperature difference ratios. We also study the heat transfer characteristics by calculating the variations of Nusselt numbers on hot and cold walls.

2. Statement of the problem

A schematic of the system considered in this paper is shown in Fig. 1. The system consists of a cube with sides of length L, within which another cubic solid body with sides of length W is centered. A cubic conducting body has a thermal conductivity of k_s and generates uniform heat per unit volume of $\dot{q}$. The temperatures of the left- and right-side walls are maintained T_h and T_c, respectively. The bottom, top, front- and rear-side walls are adiabatic. In this study, we assume that the flow within an enclosure is steady and laminar, and the radiation effects are assumed to be negligible. The fluid properties are also assumed to be constant, except for the density in the buoyancy term that follows the Boussinesq approximation. The gravitational acceleration acts parallel to the isothermal walls.

3. Analysis

The analysis is based on the steady, three-dimensional continuity, momentum, and energy equations in a dimensionless form. The conservative form of the dimensionless governing equations for fluids can be expressed as follows:

$$\frac{\partial u}{\partial x}+\frac{\partial v}{\partial y}+\frac{\partial w}{\partial z}=0 \tag{1}$$

$$\frac{\partial}{\partial x}(uu)+\frac{\partial}{\partial y}(uv)+\frac{\partial}{\partial z}(uw) = Pr\left(\frac{\partial^2 u}{\partial x^2}+\frac{\partial^2 u}{\partial y^2}+\frac{\partial^2 u}{\partial z^2}\right)-\frac{\partial P}{\partial x} \tag{2}$$

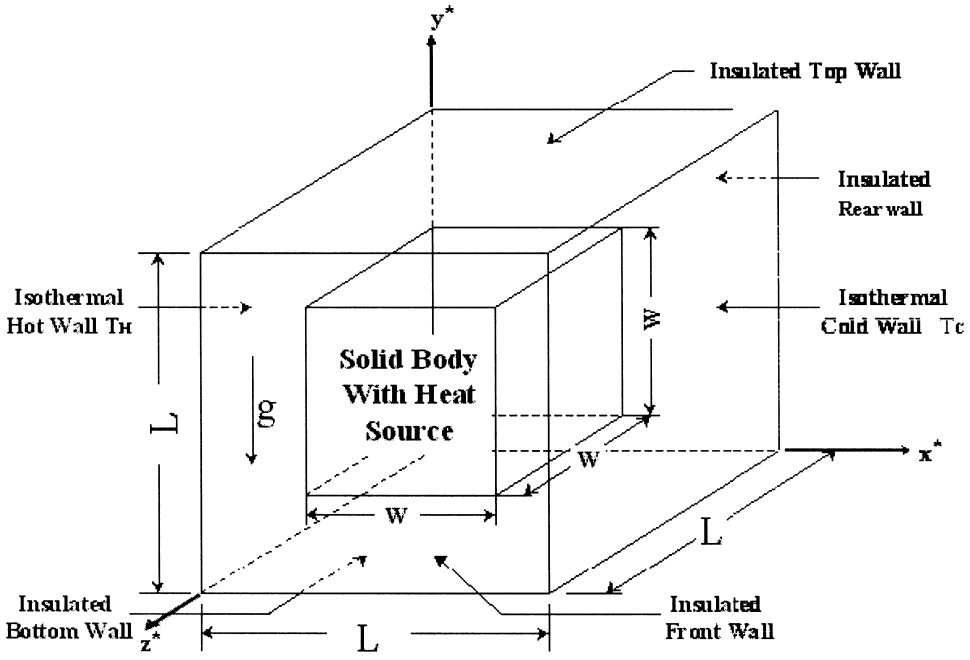

Fig. 1. A schematic of the system.

$$\frac{\partial}{\partial x}(uv)+\frac{\partial}{\partial y}(vv)+\frac{\partial}{\partial z}(vw) = Pr\left(\frac{\partial^2 v}{\partial x^2}+\frac{\partial^2 v}{\partial y^2}+\frac{\partial^2 v}{\partial z^2}\right)-\frac{\partial P}{\partial y}+Ra\,Pr\,\theta \tag{3}$$

$$\frac{\partial}{\partial x}(uw)+\frac{\partial}{\partial y}(vw)+\frac{\partial}{\partial z}(ww) = Pr\left(\frac{\partial^2 w}{\partial x^2}+\frac{\partial^2 w}{\partial y^2}+\frac{\partial^2 w}{\partial z^2}\right)-\frac{\partial P}{\partial z} \tag{4}$$

$$\frac{\partial}{\partial x}(u\theta)+\frac{\partial}{\partial y}(v\theta)+\frac{\partial}{\partial z}(w\theta)=\frac{\partial^2\theta}{\partial x^2}+\frac{\partial^2\theta}{\partial y^2}+\frac{\partial^2\theta}{\partial z^2} \tag{5}$$

For a solid body, the energy equation in a dimensionless form becomes

$$\frac{\partial}{\partial x}\left(k^*\frac{\partial\theta_s}{\partial x}\right)+\frac{\partial}{\partial y}\left(k^*\frac{\partial\theta_s}{\partial y}\right)+\frac{\partial}{\partial z}\left(k^*\frac{\partial\theta_s}{\partial z}\right)+\frac{\Delta T^*}{A^*}=0 \tag{6}$$

The dimensionless variables used to create the governing equations, Eqs. (1)–(6), are defined as

$$x=\frac{x^*}{L}\quad y=\frac{y^*}{L}\quad z=\frac{z^*}{L}\quad u=\frac{u^*L}{\alpha}$$

$$v=\frac{v^*L}{\alpha}\quad w=\frac{w^*L}{\alpha}\quad P=\frac{P^*L^2}{\rho\alpha^2}\quad \theta=\frac{T-T_c}{T_h-T_c} \tag{7}$$

For the boundary conditions, the velocities are set to zero for all solid walls. The temperature boundary conditions and the conditions at the fluid/body interface are as follows

$$\text{At } x=0: \qquad \theta=1 \tag{8}$$

$$\text{At } x=1: \qquad \theta=0 \tag{9}$$

$$\text{At } y=0 \text{ and } 1: \qquad \frac{\partial\theta}{\partial y}=0 \tag{10}$$

$$\text{At } z=0 \text{ and } 1: \qquad \frac{\partial\theta}{\partial z}=0 \tag{11}$$

$$\text{At } x=\frac{1-W/L}{2} \text{ and } \frac{1+W/L}{2}: \quad \theta_s=\theta,\quad \frac{\partial\theta}{\partial x}=k^*\frac{\partial\theta_s}{\partial x} \tag{12}$$

$$\text{At } y=\frac{1-W/L}{2} \text{ and } \frac{1+W/L}{2}: \quad \theta_s=\theta,\quad \frac{\partial\theta}{\partial y}=k^*\frac{\partial\theta_s}{\partial y} \tag{13}$$

$$\text{At } z=\frac{1-W/L}{2} \text{ and } \frac{1+W/L}{2}: \quad \theta_s=\theta,\quad \frac{\partial\theta}{\partial z}=k^*\frac{\partial\theta_s}{\partial z} \tag{14}$$

The average Nusselt numbers of the hot and cold walls are calculated based on the enclosure length and the thermal conductivity of the fluid, and are expressed as follows:

For the hot wall

$$\overline{Nu_h}=-\int_0^1\int_0^1\frac{\partial\theta}{\partial x}|_{x=0}\,dy\,dz \tag{15}$$

For the cold wall

$$\overline{Nu_c}=\int_0^1\int_0^1\frac{\partial\theta}{\partial x}|_{x=1}\,dy\,dz \tag{16}$$

From the dimensionless governing equations, Eqs. (1)–(6), it can be noticed that there are five dimensionless parameters (Ra, Pr, k^*, A^*, and ΔT^* that govern the heat transfer and flow characteristics of three-dimensional natural convection in a cubic enclosure with a heat-generating cubic-conducting body.

4. Numerical procedure

The governing equations are solved numerically by means of a finite-volume method. This approach allows for the treatment of arbitrary geometries and avoids problems with metric singularities usually associated with a finite-difference method. We first integrated the differential conservation equations over a finite volume V enclosed by surface S. The volume integral for the flux vector was converted to a surface integral through the Gauss divergence theorem. The fluid and body regions were solved simultaneously by introducing a block parameter, which distinguishes a body region from a fluid region, into discretized governing equations. Thus, convection terms were automatically turned off in the body region, and the energy balance in the fluid–body interface was carefully established to make sure that the matching conditions of Eqs. (12)–(14) were satisfied. The convergence of the numerical solution was monitored by observing the energy balance, especially the Nusselt number for both walls for every time step.

For the purpose of code validation, the natural convection problem in an enclosure without a cubic body in the center of the enclosure was tested for $Ra = 10^3$, 10^4 and 10^5, respectively, using a grid size of $41 \times 41 \times 41$ in the x-, y-, and z-directions. The calculated average Nusselt numbers at the hot wall for the test cases were compared with the values calculated by Fusegi et

Table 1
Comparison of the present average Nusselt number at the hot wall with Fusegi et al.'s results for $Pr = 0.71$

Ra		10^3	10^4	10^5
$\overline{Nu}$	Fusegi et al. [8]	1.085	2.1	4.361
	Present study	1.072	2.07	4.464

al. [8]. As shown in Table 1, the calculated Nusselt numbers agree well with the values calculated by Fusegi et al. [8], and the deviation from Fusegi et al.'s results was less than 2.4%. The temperature and velocity profiles from the present calculation for $Ra = 10^5$ represented well the results obtained by Fusegi et al. [8], as shown in Figs. 2 and 3.

5. Results and discussion

After a successful benchmark test for our three-dimensional program, we investigated three-dimensional heat transfer and flow phenomena of natural convection in a vertical cubic enclosure within which a centered, cubic, heat conducting body generates heat. The grid system employed for all the calculations in this article is shown in Fig. 4, with a grid size of $51 \times 51 \times 51$ in the x-, y-, and z-directions. The grid is stretched a little toward each wall to resolve the rapid variations of flow properties. As mentioned earlier, there are five dimensionless parameters that govern the steady natural convection heat transfer and the flow of this system. In the present study, we consider the case in which a sodium fluid surrounds a heat-generating and conducting body, resulting in constant Pr, k^* and A^* values of 0.0112, 1.72, and 0.25, respectively. We calculated the cases shown in Table 2 for two Rayleigh numbers (10^3 and 10^4) and two temperature-difference ratios (2.5 and 25) to investigate their influence on the heat transfer and flow structures of the system.

Table 2
Values of Rayleigh number and temperature-difference ratio used in the present study

	Ra	ΔT^*
Case 1	10^3	2.5
Case 2	10^3	25.0
Case 3	10^4	2.5
Case 4	10^4	25.0

5.1. Case of $Ra = 10^3$

Figs. 5 and 6 show the velocity vectors and pathlines at different x-, y-, and z-planes for $Ra = 10^3$ and $\Delta T^* = 2.5$. The constant x-, y-, and z-planes are, respectively, located at the upper, middle, and lower parts of Figs. 5 and 6. As shown in the constant z-planes, the flow circulates in the clockwise direction, due to the presence of hot and cold walls on the left and right sides, respectively. The velocity vectors at the $z = 0.125$ and 0.875 planes corresponding to the center plane of the front and rear channels are similar to the flow in a cubic enclosure without a heat-generating

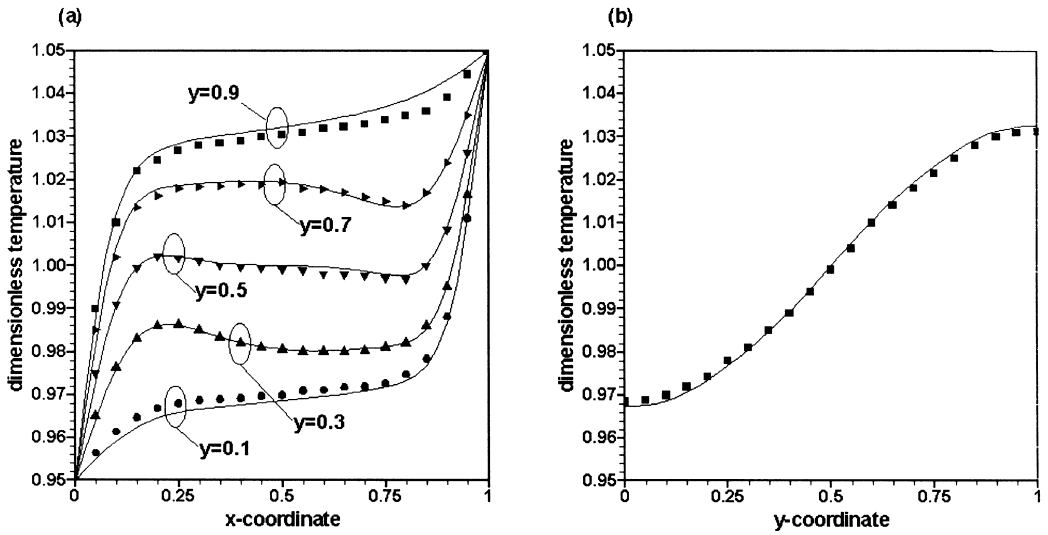

Fig. 2. Comparison of the present results (shown in symbols) for temperature profiles in the symmetry plane of $z = 0.5$ with results of Fusegi et al. [8] (shown in solid curves) for $Ra = 10^5$: (a) results at various heights, (b) results at $x = 0.5$.

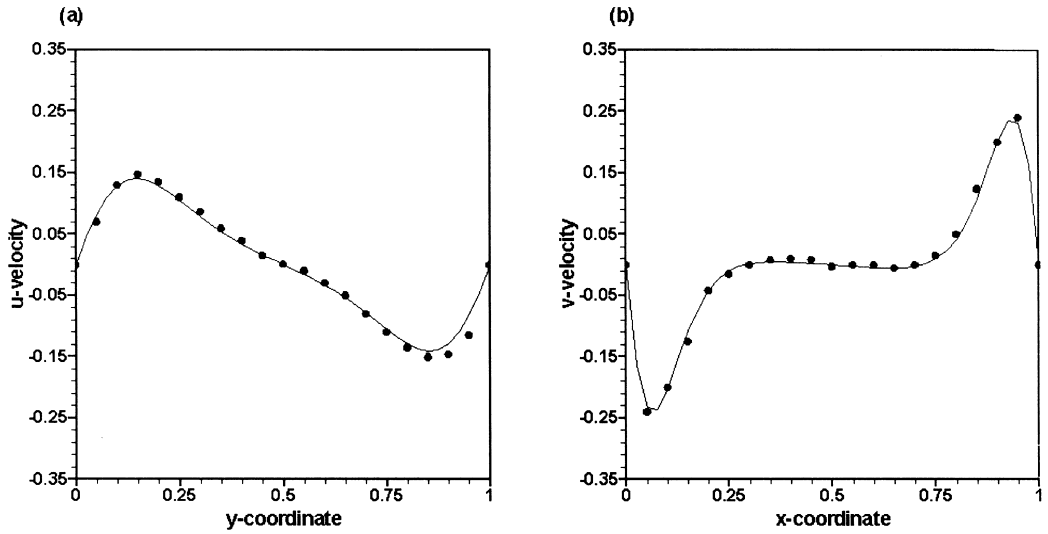

Fig. 3. Comparison of the present results (shown in solid curves) for temperature profiles in the symmetry plane of $z = 0.5$ with results of Fusegi et al. [8] (shown in symbols) for $Ra = 10^5$: (a) $x = 0.5$, (b) $y = 0.5$.

and conducting body, which forms a single shell in the enclosure. The velocity vectors at the $z = 0.5$ plane corresponding to the center z-plane of the enclosure have different pattern than those at $z = 0.125$ and 0.875, due to the presence of a conducting body. Due to the main circulating flow that moves in the clockwise direction, the velocity vectors generally move from bottom to top at the $x = 0.125$ plane (center plane of the left channel), and from top to bottom at the $x = 0.875$ plane (center plane of the right chan-

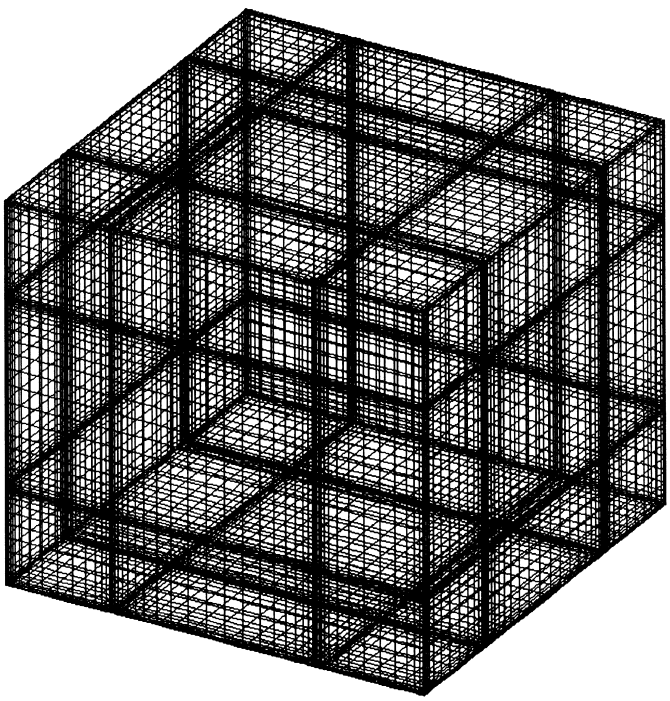

Fig. 4. Grid distribution of computational domain.

nel). The flow at the $x = 0.5$ plane (center x-plane of the enclosure) shows a more complex pattern than that at the left and right channels. Due to the presence of a cubic conducting body, the flow rises generally from bottom to top and forms recirculating flows both at the top corners of the enclosure and at the top corners of the conducting body. Similar to the flow at constant x-planes, the flow at the $y = 0.125$ plane (center plane of the bottom channel) moves from right to left, and that at the $y = 0.875$ plane (center plane of the top channel) directs from left to right, because the main flow circulates in the clockwise direction. The flow at the $y = 0.5$ plane (center y-plane of the enclosure) generally moves from left to right with a more complex pattern, compared to the flow at the bottom and the top channels, and forms vortices at the corners on the right side of the conducting body.

Figs. 7–9 show the iso-velocity contours of u-, v-, and w-velocity components at different constant planes for $Ra = 10^3$ and $\Delta T^* = 2.5$. Because the circulating flow moves mainly in the clockwise direction, the u-velocity has large positive and negative values at the top and bottom channels, respectively, while the v-velocity has large positive and negative values at the right and

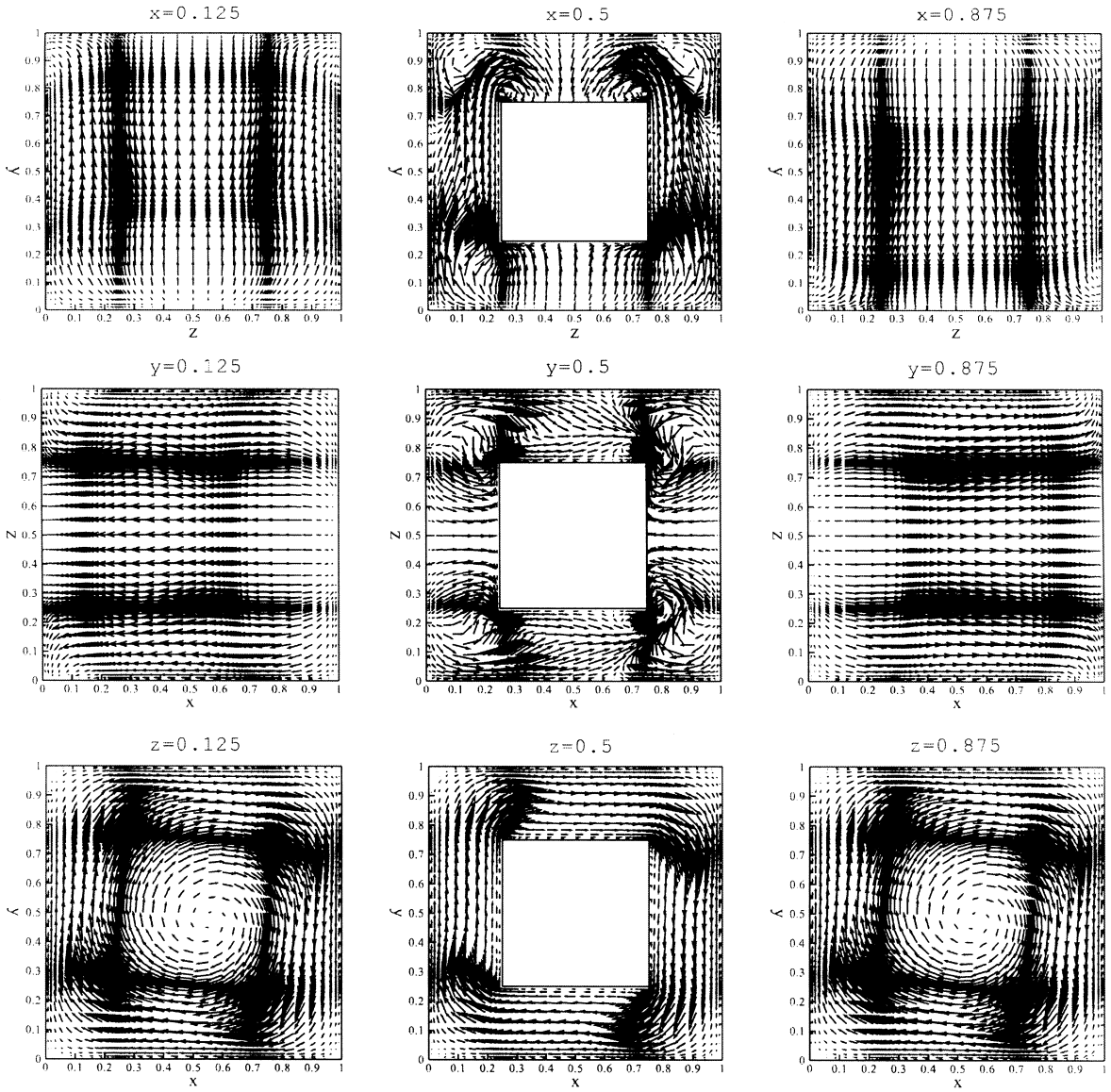

Fig. 5. Velocity vectors for different x-, y-, and z-planes for $Ra = 10^3$ and $\Delta T^* = 2.5$.

left channels, respectively. The w-velocity generally has smaller values than do the u- and v-velocities, but shows a more complex pattern, compared to u- and v-velocity contours. The u-, v-, and w-velocities have large variations in the z-direction, due to the presence of the conducting body. Thus, the u-, v-, and w-velocities show very complex three-dimensionalities of flow in an enclosure with the presence of the conducting body, compared to the case without the conducting body of Fusegi et al. [8].

Fig. 10 shows isotherms at different constant planes for $Ra = 10^3$ and $\Delta T^* = 2.5$. At the $z = 0.125$ and 0.875 planes, the isotherms at the upper part lean very slightly on the cold wall, and those at the lower part likewise lean very slightly on the hot wall, due to the presence of a small fluid flow circulating in the clockwise direction. However, because the heat is transferred from the conducting body to the fluid at the $z = 0.5$ plane, the isotherms at the left and right channels of the $z = 0.5$ plane have lower and higher gradients, respectively, than the isotherms at the $z = 0.125$ and 0.875 planes. Because the thermal conductivity of the body is greater than that of fluid, the isotherms in the conducting body lean more to the cold wall than

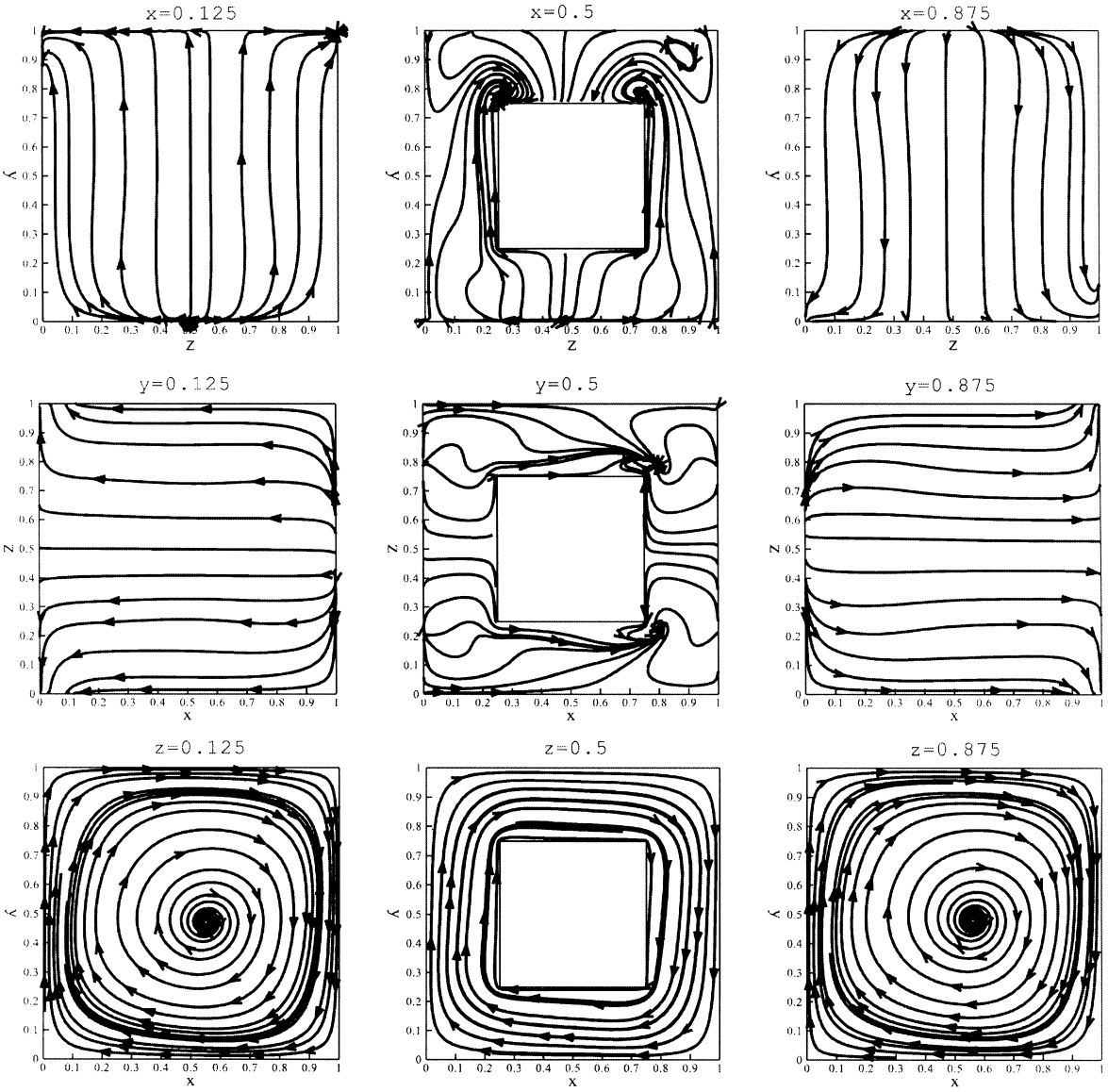

Fig. 6. Pathlines for different x-, y-, and z-planes for $Ra = 10^3$ and $\Delta T^* = 2.5$.

those in the fluid at the $z = 0.5$ plane. Isotherms at the $y = 0.125$ plane are almost parallel to the z-axis. The interval between isotherms is almost uniform, showing conduction dominance at the bottom channel. The iostherms at the $y = 0.5$ plane are similar to those at the $z = 0.5$ plane. The thermal gradients at the $y = 0.5$ plane increase with increasing x-distance. Because the heat is transferred to the fluid from the hot wall and the conducting body and the flow circulates in the clockwise direction, the isotherms at the $y = 0.875$ plane have lower and higher thermal gradients at the left and right channels, respectively. At the constant x-planes, due to the circulating flow in the clockwise direction and the heat transferred from the hot wall and the conducting body to the fluid, the values of isotherms decrease with increasing x-distance from the hot wall and increase with increasing y-distance from the bottom wall. The isotherms at the constant x-planes show large variations in shape in the z-direction. This results represent stronger three-dimensionalities of the present problem with the presence of a cubic conducting body than natural convection without a conducting body.

Figs. 11 and 12 show the velocity vectors and path-

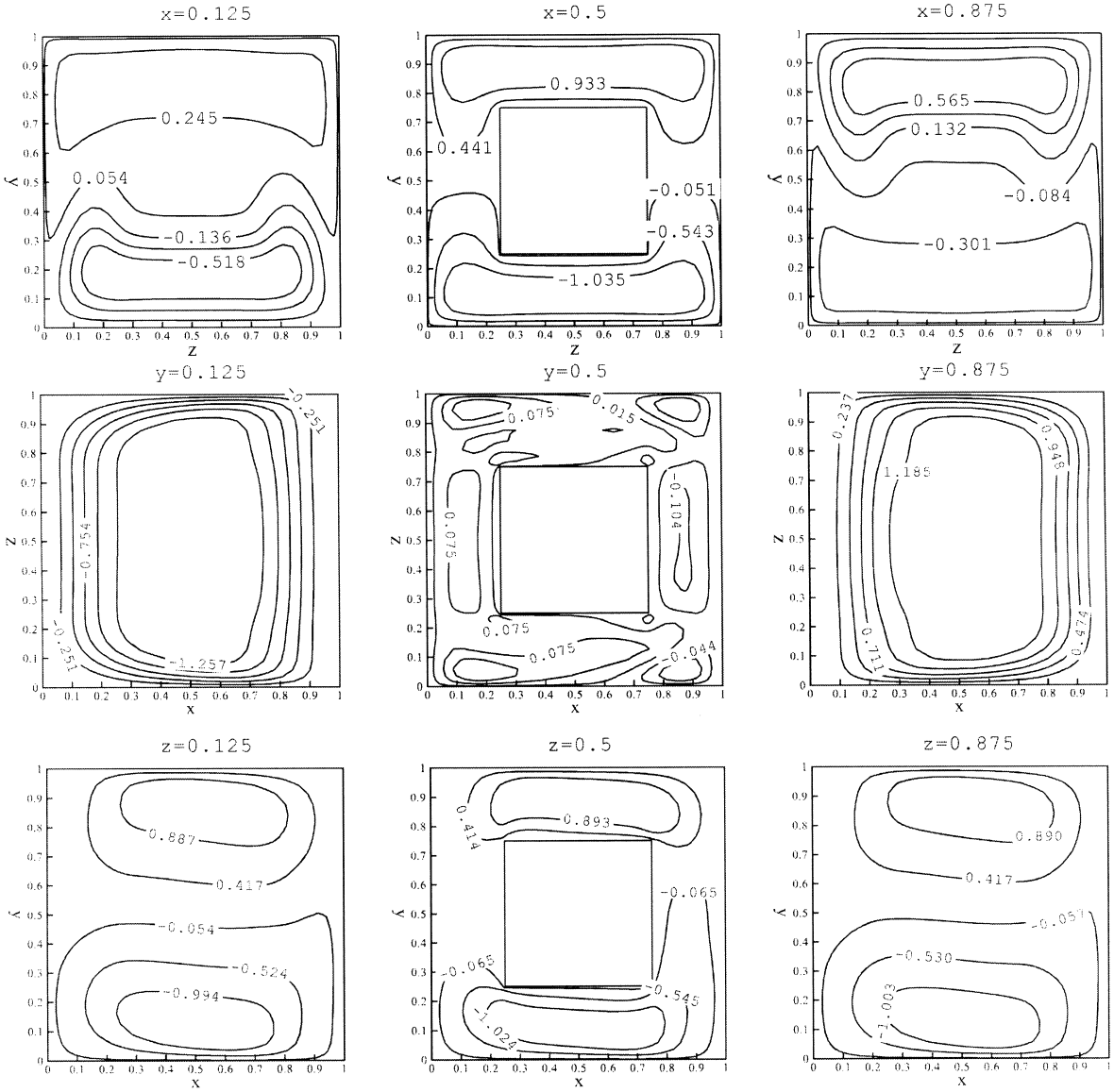

Fig. 7. u-Velocity contours for different x-, y-, and z-planes for $Ra = 10^3$ and $\Delta T^* = 2.5$.

lines at different constant planes for $Ra = 10^3$ and $\Delta T^* = 25$. When ΔT^* is increased to 25, the fluid temperature at the left channel becomes higher than the hot wall temperature, due to increasing heat transfer from the conducting body. Thus, the flow for case 2 shows a much different pattern from that for case 1. At the $z = 0.125$ and 0.875 planes, the flow close to the hot wall moves downward and forms the recirculating flow in the counterclockwise direction in addition to the main circulating flow in the clockwise direction. Thus, two cells circulate in the opposite directions, compared to the one cell formed in a cubic enclosure without a conducting body. At the $z = 0.5$ plane, the main flow circulates in the clockwise direction. However, the vortex at the left channel is divided into two parts at the top and bottom corners, due to the presence of a conducting body. Because of heat transfer from the body, small vortices circulate in the clockwise direction next to the body at the right channel. The flow at the $x = 0.125$ plane generally moves upwards around $z = 0.5$. However, when the flow approaches the wall at $z = 0$ and 1, the flow at the

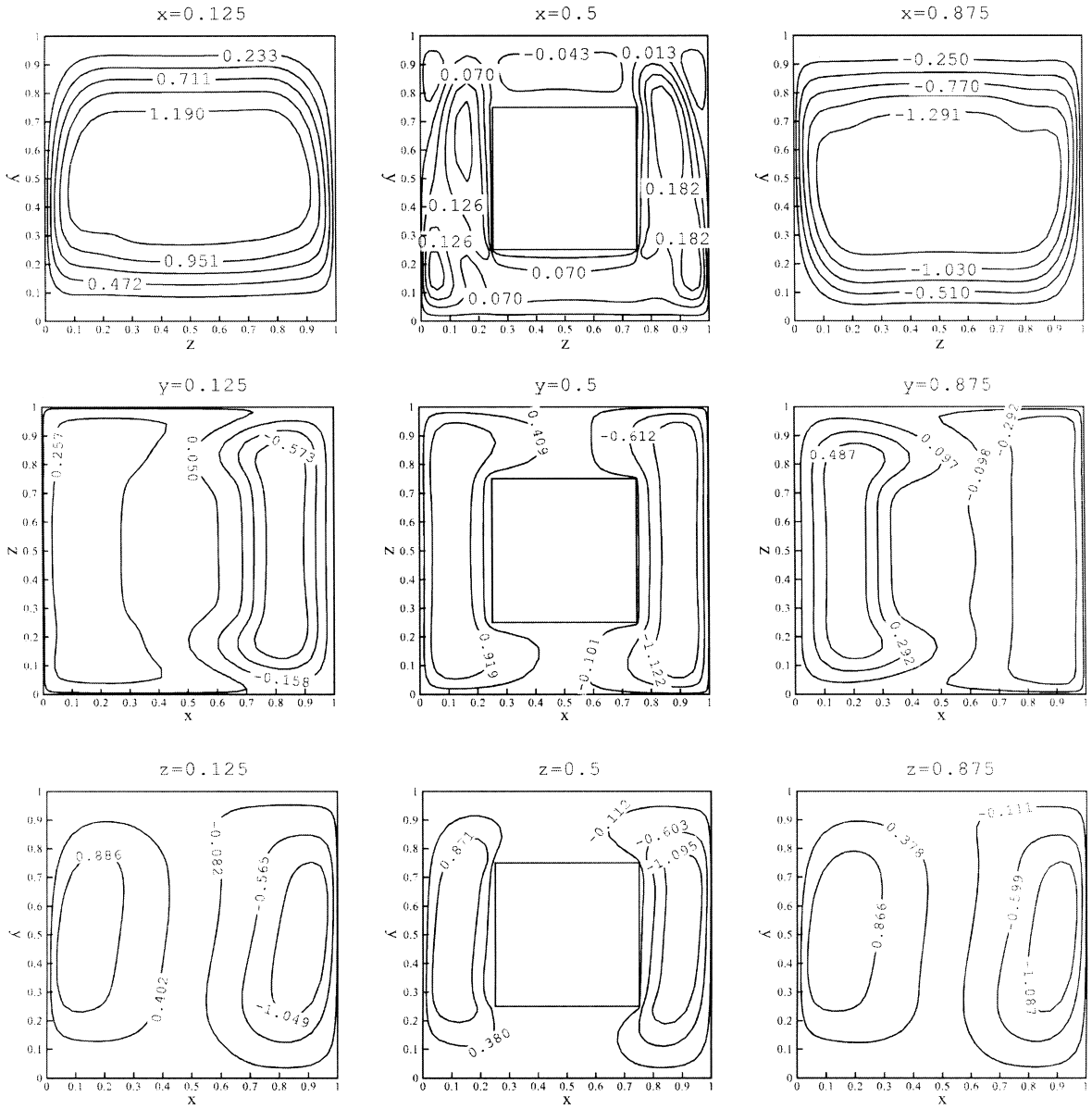

Fig. 8. v-Velocity contours for different x-, y-, and z-planes for $Ra = 10^3$ and $\Delta T^* = 2.5$.

upper part moves downward, due to the effects of the recirculating flow at the left channel, and shows a different flow pattern from that for case 1. The flow at $x = 0.5$ generally moves upward and forms a recirculating flow around the top right and left corners of the conducting body. However, the vortices formed at the top right and left corners of the enclosure (as observed in case 1) vanish, due to an increasing upward flow with increasing heat transfer to the fluid from the conducting body. The flow at $x = 0.875$ generally moves downward, similar to case 1. The flow at $y = 0.125$ (bottom channel) generally directs from right to left. The magnitude of the flow velocity close to the left wall becomes smaller and changes its direction from left to right, due to the recirculating flow in the counterclockwise direction at the left channel. The main flow at $y = 0.875$ (top channel) moves from left to right, but the flow at the left channel directs from right to left at the left channel, due to the recirculating flow at the left channel. The flow at $y = 0.5$ generally directs from left to right, similar to case 1.

Fig. 13 shows the isotherms at different x-, y-, and z-planes for $Ra = 10^3$ and $\Delta T^* = 25$. When ΔT^* is increased to 25, the temperature of the fluid and the

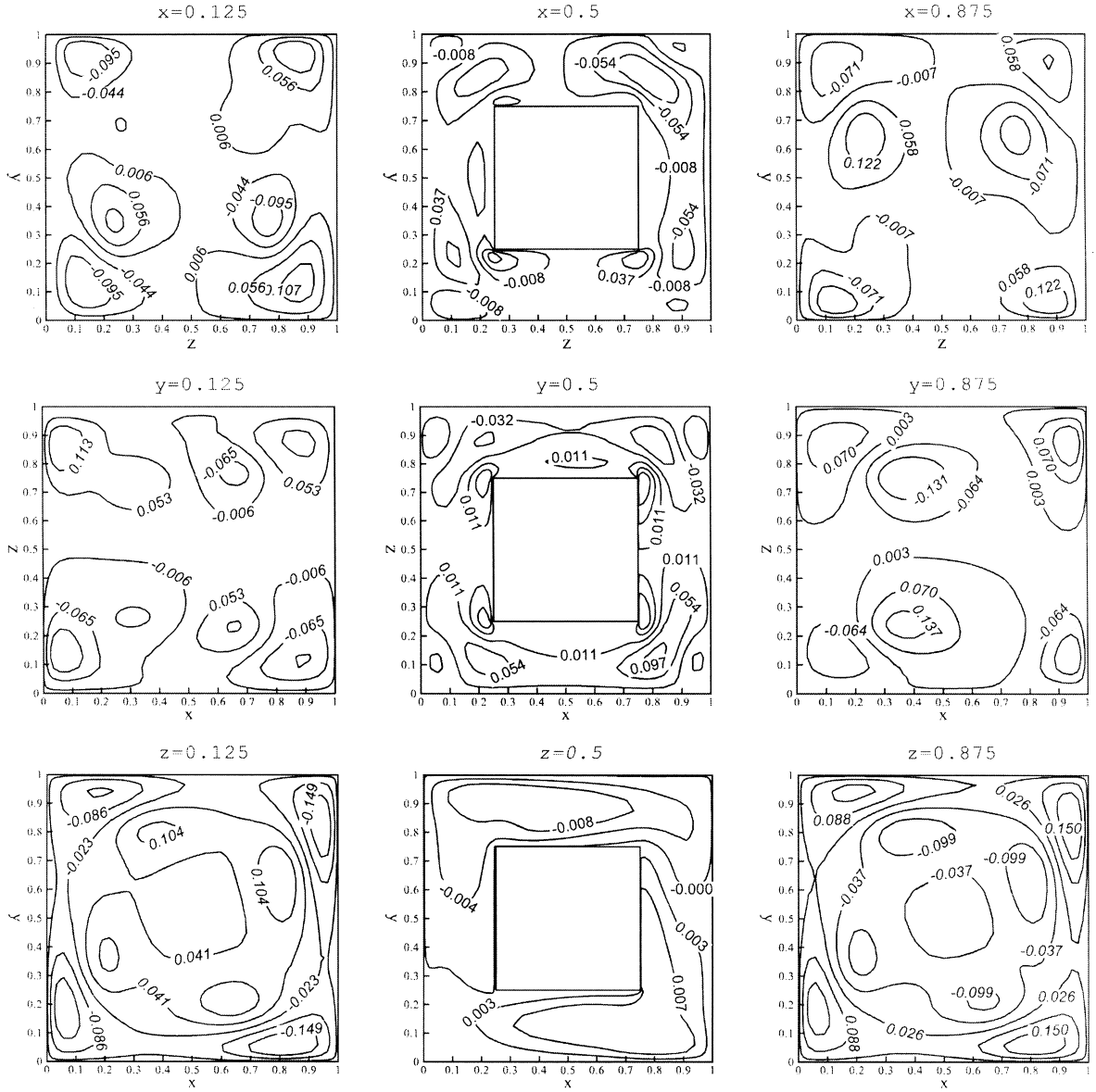

Fig. 9. w-Velocity contours for different x-, y-, and z-planes for $Ra = 10^3$ and $\Delta T^* = 2.5$.

body increases with increasing heat generation at the conducting body. The fluid temperature at the left channel becomes higher than the hot wall temperature with a lower gradient, while the fluid temperature at the right channel is low with a denser gradient. The maximum temperature at the conducting body is higher than the hot wall temperature and is located close to the center of the body. The heat transfer and fluid flow characteristics of the enclosure become dominated by the temperature difference caused by the heat source at $\Delta T^* = 25$, resulting in different isotherm patterns from that for case 1.

5.2. Case of $Ra = 10^4$

Fig. 14 shows the velocity vectors, pathlines, and isotherms at different z-planes for $Ra = 10^4$ and $\Delta T^* = 2.5$. The flow for case 3 of $Ra = 10^4$ and $\Delta T^* = 2.5$ smoothly circulates in the clockwise direction, similar to that for case 1 of $Ra = 10^3$ and $\Delta T^* = 2.5$. However, if the circulating flow meets the corner of the conducting body when the velocity magnitude increases with an increasing Rayleigh number, the flow separates from the corner and is reattached to the surface of the body, forming four vortices on the

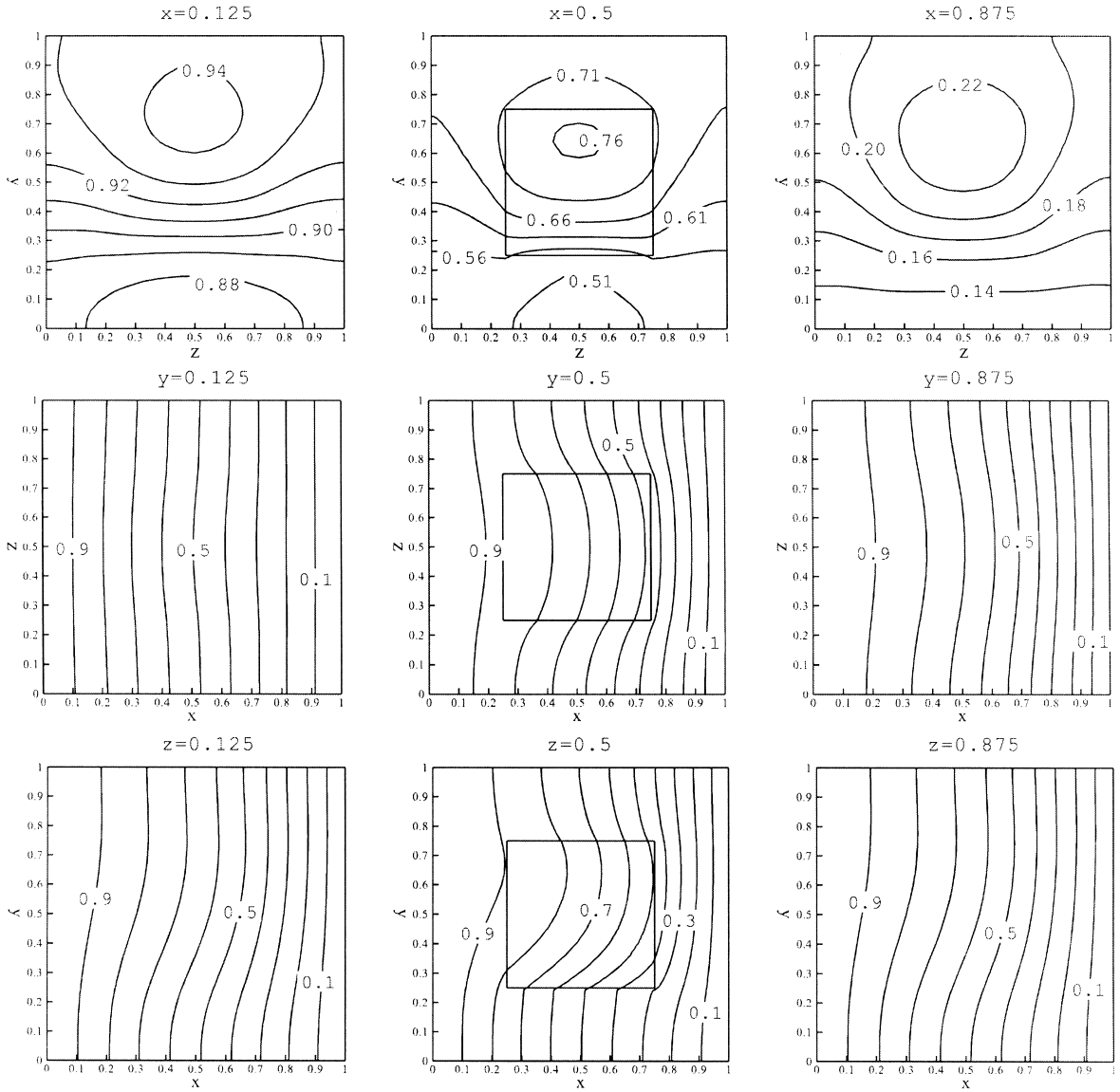

Fig. 10. Isotherms for different x-, y-, and z-planes for $Ra = 10^3$ and $\Delta T^* = 2.5$.

surface of the conducting body. Thus, a flow pattern for case 3 is different from that for case 1. The corner vortices in the four corners of the enclosure are also observed, due to an increase in the velocity with an increase in the Rayleigh number. When the Rayleigh number is increased to 10^4, the isotherms move in the clockwise direction with increasing circulating flow, resulting in a dense gradient around the top right and bottom left corner. When the isotherms at $z = 0.125$ and 0.5 are compared, the isotherms in the conducting body have a slightly denser gradient than that in the fluid, because the thermal conductivity of the body is larger than that of the fluid.

Fig. 15 shows the velocity vectors, pathlines, and isotherms at different z-planes for $Ra = 10^4$ and $\Delta T^* = 25$. At the $z = 0.125$ and 0.875 planes, the size of the main flow circulating in the clockwise direction decreases, and the size of the vortex in the top left corner increases, due to an increase in velocity with an increasing Rayleigh number. At the $z = 0.5$ plane, vortices form at the top left corner and the bottom surface of the conducting body, which are not present in case 2 of $Ra = 10^3$ and $\Delta T^* = 25$. The size of the

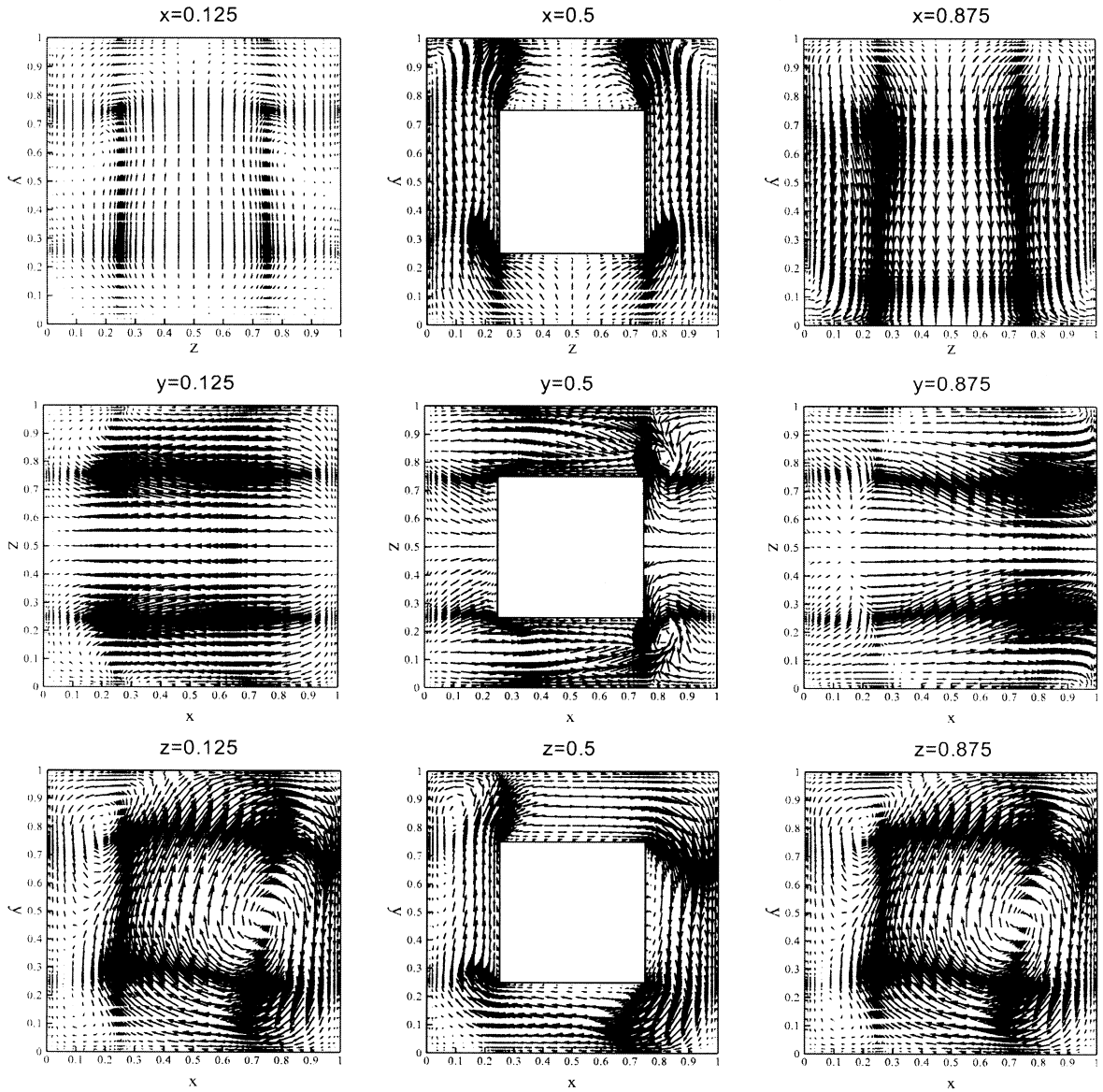

Fig. 11. Velocity vectors for different x-, y-, and z-planes for $Ra = 10^3$ and $\Delta T^* = 25$.

vortex on the right-side surface of the body also increases, compared to case 2. The general shape of the isotherms for case 4 is similar to that for case 2 and is mainly governed by the heat transfer from the conducting body. The values of the isotherms for case 4 are slightly lower than those for case 2 because more heat is transferred to the cold wall, due to an increase in convection with an increasing Rayleigh number.

5.3. Local and average Nusselt numbers

Fig. 16 shows the distribution of local Nusselt numbers at the hot and cold walls for case 1 ($Ra = 10^3$ and $\Delta T^* = 2.5$). The general shape of the local Nusselt number distribution at the hot and cold walls is similar to the isotherm distribution at the $x = 0.125$ and 0.875 planes shown in Fig. 10 because the local Nusselt number is determined from the gradient of the isotherms normal to the hot and cold walls. The fluid temperature at the left channel increases due to heat transfer from the hot wall and the body while the fluid moves upward at the left channel. Thus, the temperature difference between the hot wall ($\theta = 1$) and the fluid at the left channel decreases, and the local Nus-

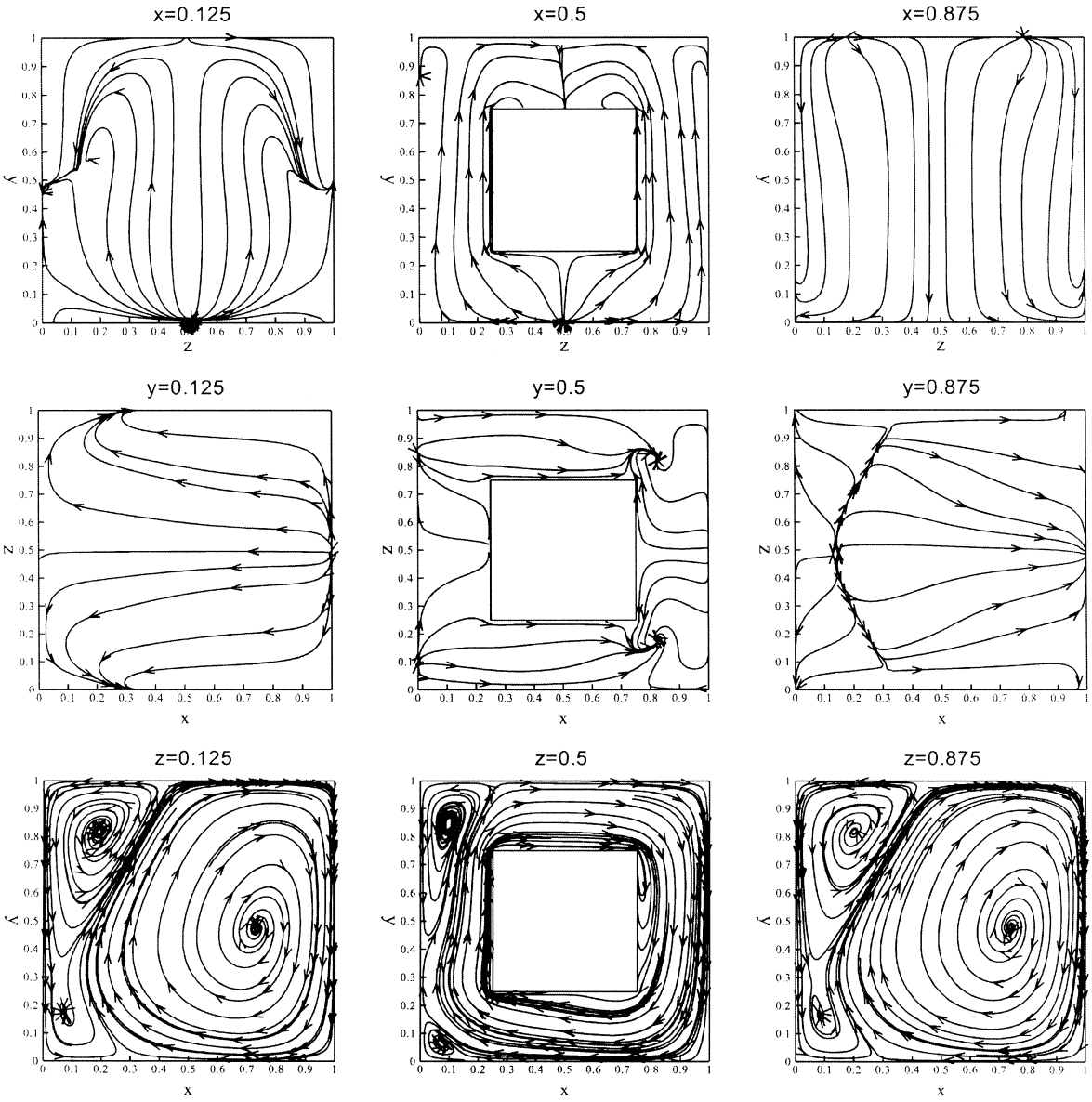

Fig. 12. Pathlines for different x-, y-, and z-planes for $Ra = 10^3$ and $\Delta T^* = 25$.

selt number decreases with increasing y-distance from the bottom wall. The cubic conducting body with heat generation is located at the center of a cubic enclosure, as shown in Fig. 1. Thus, the fluid at $0.25 \leq z \leq 0.75$ receives more heat from the conducting body than the fluids located at $0 \leq z \leq 0.25$ and $0.75 \leq z \leq 1$, due to its direct contact with the conducting body, resulting in a smaller temperature difference at $0.25 \leq z \leq 0.75$ than at $0 \leq z \leq 0.25$ and $0.75 \leq z \leq 1$. Thus, the local Nusselt number around $z = 0$ (front wall) and $z = 1$ (rear wall) is larger than that around $z = 0.5$, proving three-dimensional heat transfer characteristics of the system. While the fluid moves downward at the right channel, the fluid temperature decreases, due to heat transfer to the cold wall, and the temperature difference between the cold wall and the fluid decreases. Thus, the local Nusselt number at the cold wall increases with increasing y-distance from the bottom wall. The local Nusselt number at the cold wall also varies along the z-direction. The fluid temperature and the temperature difference between the fluid and the cold wall at $0.25 \leq z \leq 0.75$ are larger than those at $0 \leq z \leq 0.25$ and $0.75 \leq z \leq 1$. Thus, the local Nusselt number at $0.25 \leq z \leq 0.75$ is larger than that at $0 \leq z \leq 0.25$ and $0.75 \leq z \leq 1$. This local Nusselt number distribution at the hot and cold walls shows stronger three-dimensionalities of the present problem than the

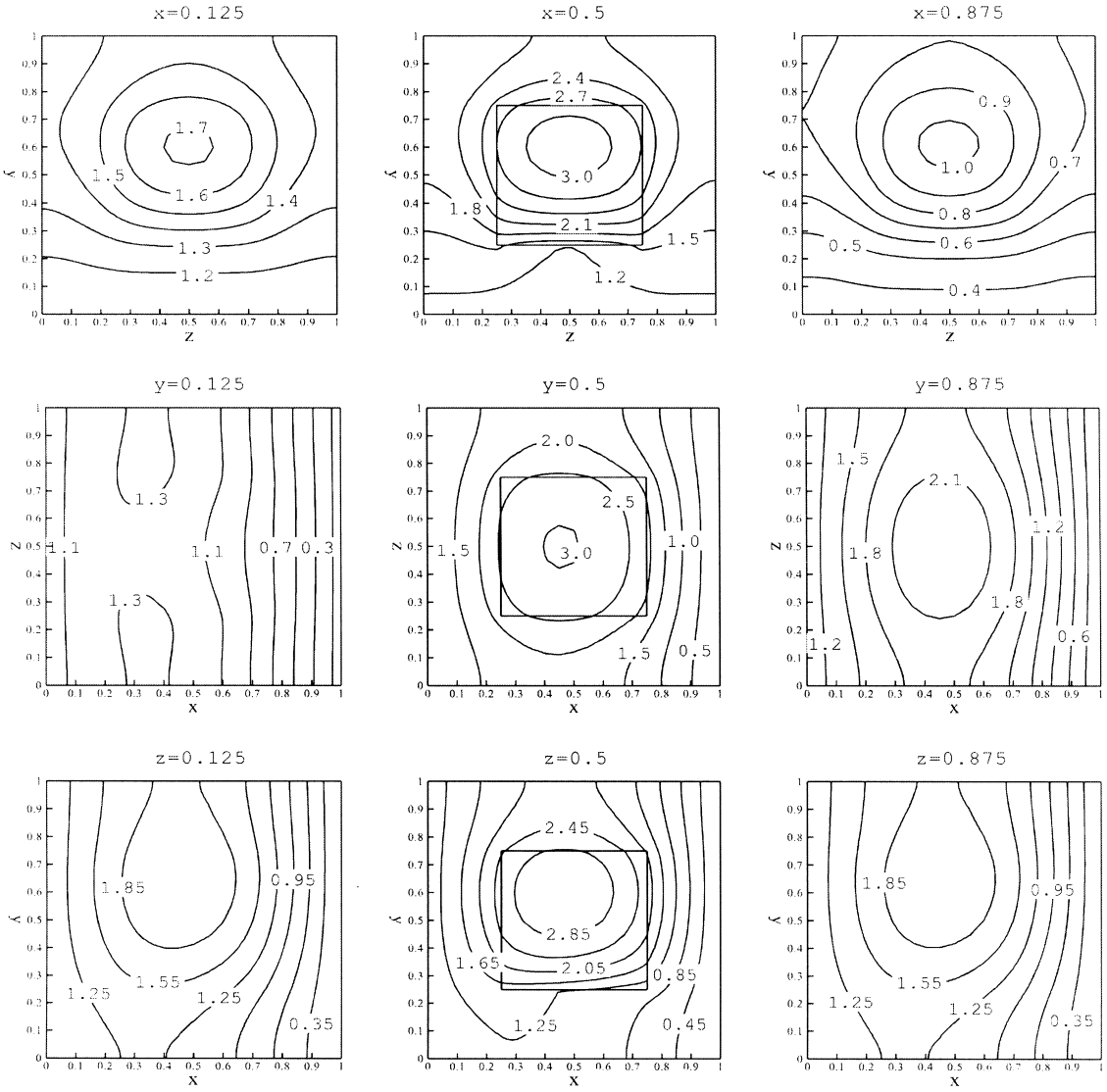

Fig. 13. Isotherms for different x-, y-, and z-planes for $Ra = 10^3$and $\Delta T^* = 25$.

three-dimensional natural convection in a cubic enclosure without a conducting body.

Fig. 17 shows the distribution of local Nusselt numbers at the hot and cold walls for case 2 ($Ra = 10^3$ and $\Delta T^* = 25$). When ΔT^* is increased to 25 from 2.5 of case 1, the fluid temperature at the hot wall becomes higher than the hot wall temperature. Thus, the heat is transferred from the fluid to the hot wall, resulting in a negative local Nusselt number at the hot wall. Similar to case 1, the local Nusselt number decreases with increasing y-distance from the bottom wall, meaning that the heat transferred from the fluid to the hot wall increases with increasing y-distance from the bottom wall. The position of the minimum negative (maximum absolute) local Nusselt number is located around $y = 0.63$, due to the heat transfer from the body to the circulating flow. The local Nusselt number along the z-direction for case 2 has a pattern similar to that for case 1, showing a larger local Nusselt number around the front and rear walls than around the center. The local Nusselt number distribution at the cold wall for case 2 is similar to that for case 1. However, the magnitude of the local Nusselt number at the cold wall for case 2 is larger than that for case 1, due to increasing heat transfer from the conducting body. The position of the maximum local

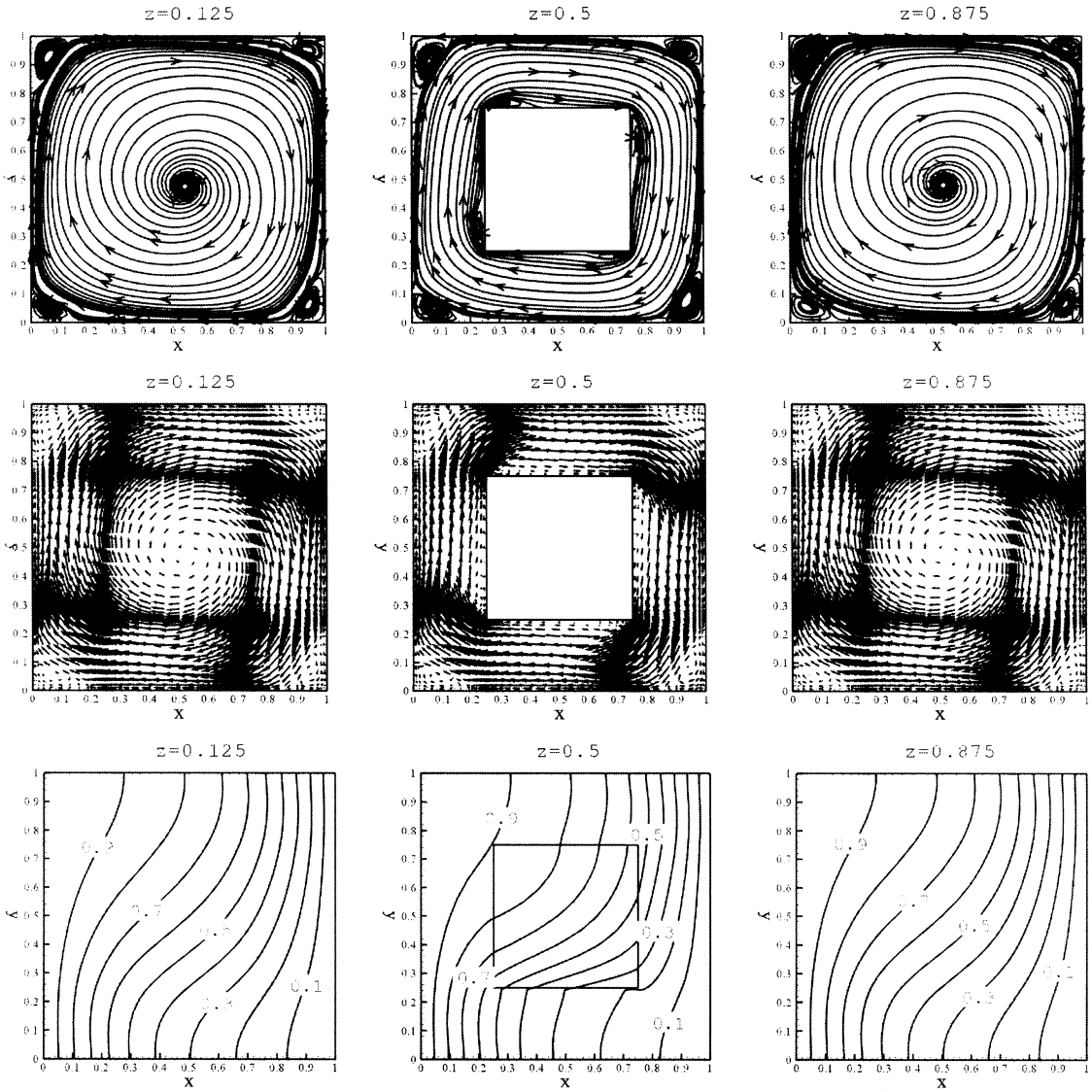

Fig. 14. Pathlines, velocity vectors and isotherms for different x-, y-, and z-planes for $Ra = 10^4$ and $\Delta T^* = 2.5$.

Nusselt number at the cold wall is around $y = 0.63$; this position is similar to that of the hot wall.

Fig. 18 shows the local Nusselt number distribution at the hot and cold walls for case 3 ($Ra = 10^4$ and $\Delta T^* = 2.5$). The general trend for the variation of the local Nusselt numbers at the hot and cold walls along the y-direction for case 3 is similar to that for case 1. With increasing y-distance from the bottom wall, the local Nusselt numbers at the hot wall decrease and those at the cold wall increase. When the Rayleigh number is increased from 10^3 for case 1 to 10^4 for case3, the convection effects increase with increasing magnitude of velocity. Thus, the local Nusselt numbers at the hot and cold walls for case 3 are generally larger than those for case 1, due to an increase in convection with an increase in Rayleigh number. When $\Delta T^* = 2.5$, the amount of heat transfer rate from the conducting body is small. If the Rayleigh number is increased from 10^3 to 10^4 for $\Delta T^* = 2.5$, the effects of convective heat transfer due to the temperature differ-

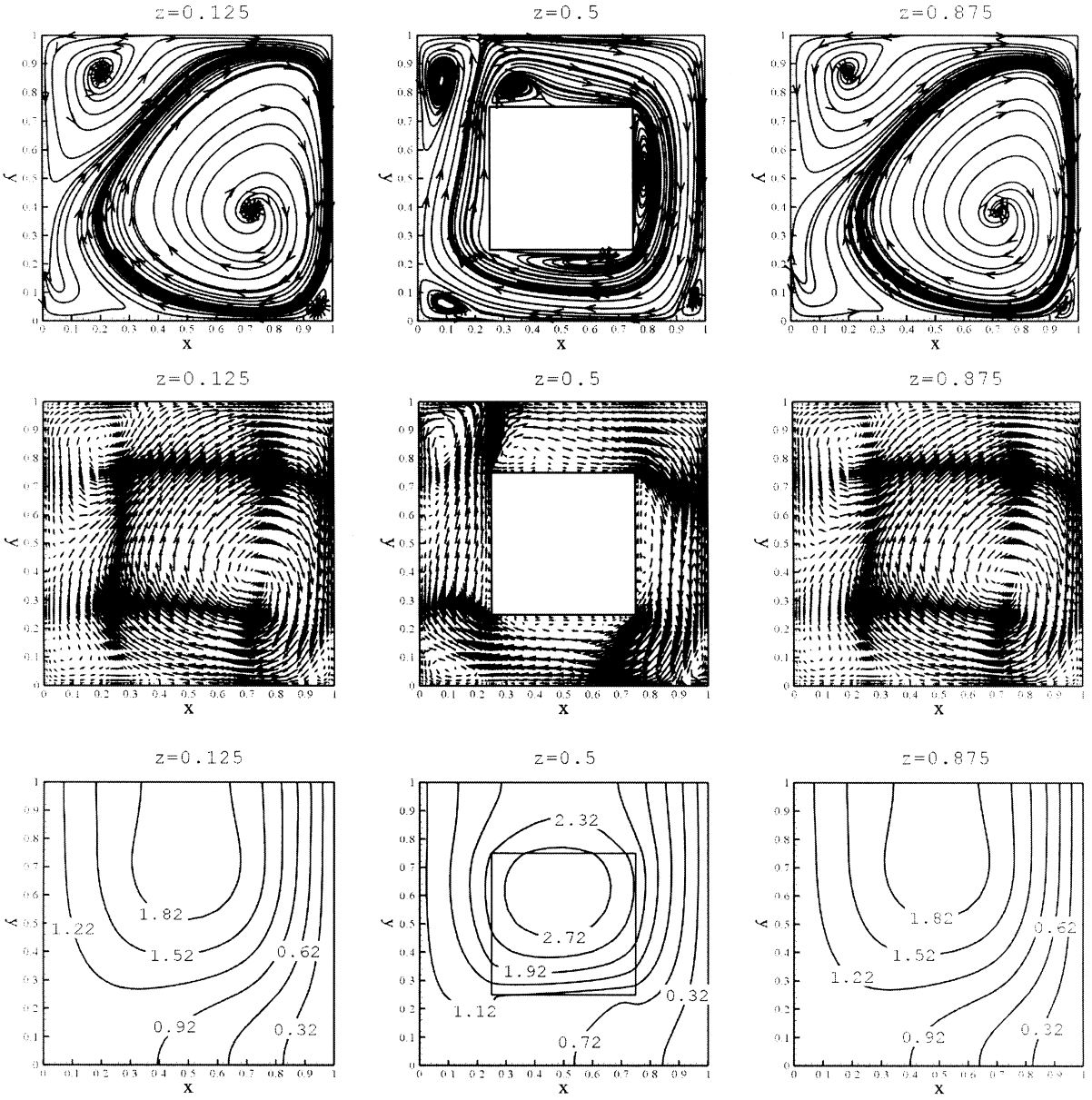

Fig. 15. Pathlines, velocity vectors and isotherms for different x-, y-, and z-planes for $Ra = 10^4$ and $\Delta T^* = 25$.

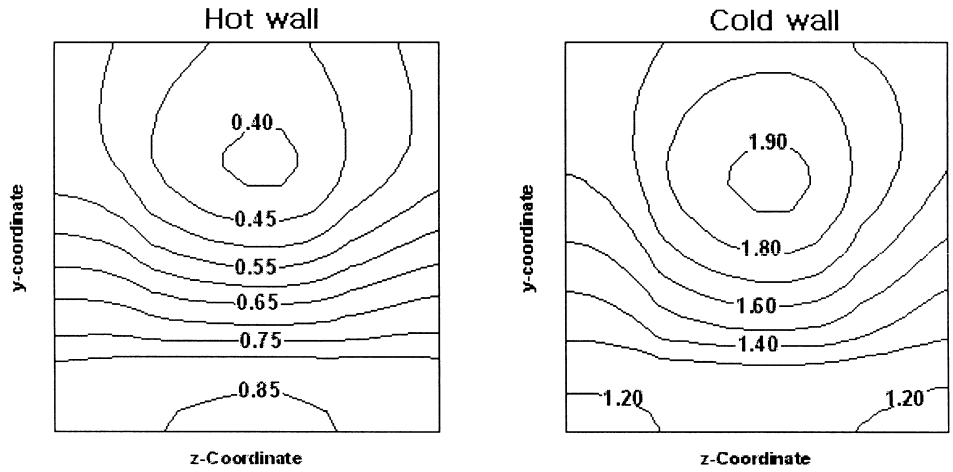

Fig. 16. Local Nusselt number at the hot and cold walls for $Ra = 10^3$ and $\Delta T^* = 2.5$.

ence between the hot and cold walls are larger than those due to temperature difference caused by the heat source of the conducting body. Thus, the local Nusselt numbers at the hot and cold walls along the z-direction for case 3 show smaller variation than that for case 1.

Fig. 19 shows the local Nusselt number distribution at the hot and cold walls for case 4 ($Ra = 10^4$ and $\Delta T^* = 25$). When ΔT^* is increased to 25 for $Ra = 10^4$, the heat transfer in the enclosure is mainly governed by the heat transfer from the conducting body. Thus, the general pattern of the local Nusselt number distribution at the hot and cold walls for case 4 is similar to that for case 2. The main difference between case 2 and case 4 is that, with increasing convective heat transfer due to the temperature difference between the hot and cold walls, the value of the local Nusselt number for case 4 is larger than that for case 2. The position of the maximum absolute local Nusselt number at the hot and cold walls for case 4 moves somewhat upward, compared to the case 2, due to the increased circulating velocity.

The average Nusselt number at the hot and cold walls is obtained by integrating the local Nusselt number according to Eqs. (15) and (16), as given in Table 3. At $\Delta T^* = 2.5$ in cases 1 and 3, the average Nusselt number at the hot and cold walls has positive values, meaning that heat is transferred from the hot wall to the fluid and from the fluid to the cold wall. As ΔT^* is increased to 25 in cases 2 and 4, the average Nusselt number at the hot wall has negative values, meaning that heat is transferred from the fluid to the hot wall. The convection and heat transfer increase with increas-

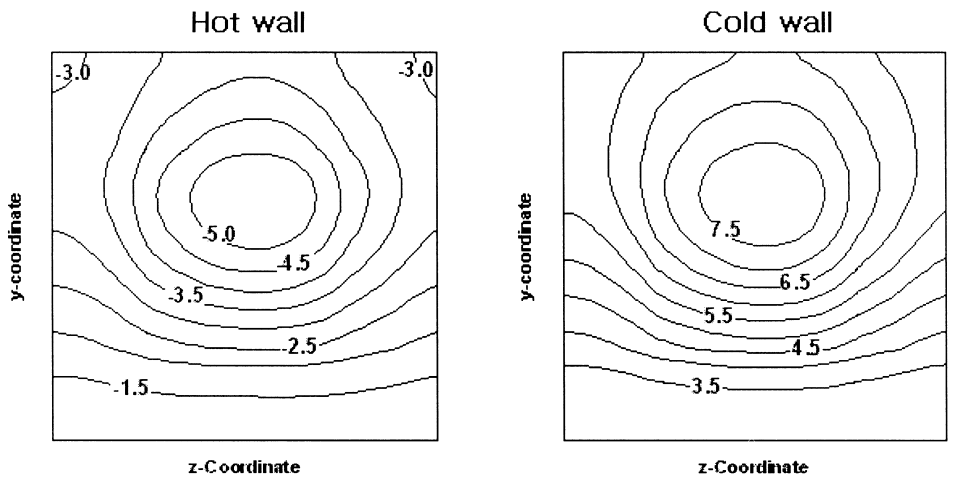

Fig. 17. Local Nusselt number at the hot and cold walls for $Ra = 10^3$ and $\Delta T^* = 25$.

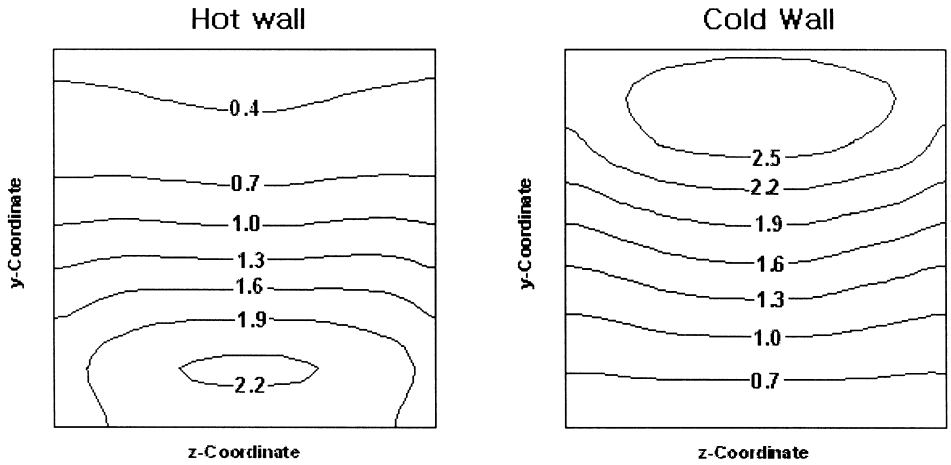

Fig. 18. Local Nusselt number at the hot and cold walls for $Ra = 10^4$ and $\Delta T^* = 2.5$.

ing Rayleigh number and ΔT^*. Thus, the average Nusselt number increases with increasing Rayleigh number and ΔT^*. As shown in Table 3, the present three-dimensional results are compared with two-dimensional ones, and show big differences between two results, due to the three-dimensionalities of the present problem with the presence of the body with an enclosure.

6. Summary and conclusion

A numerical study has been conducted to investigate the steady, three-dimensional heat transfer and flow characteristics of natural convection in a vertical cubic enclosure when a temperature difference exists across the enclosure and, at the same time, when a cubic conducting body generates heat within the cubic enclosure. The following summarizes the notable features observed in this study.

1. A computer program was developed to calculate the three-dimensional conjugate heat transfer problem of natural convection and conduction heat transfer.
2. The flow and isotherm distributions show very complex three-dimensional patterns, owing to the presence of a conducting body and heat transfer from the conducting body. The presence of a conducting body results in more three-dimensionalities in the transverse direction for both fluid flow and heat transfer.
3. At $\Delta T^* = 2.5$, the local Nusselt numbers at the hot and cold walls for $Ra = 10^3$ vary significantly in the z-direction, due to the heat transfer from the conducting body. However, when the Rayleigh number is increased to the value of 10^4, the convective

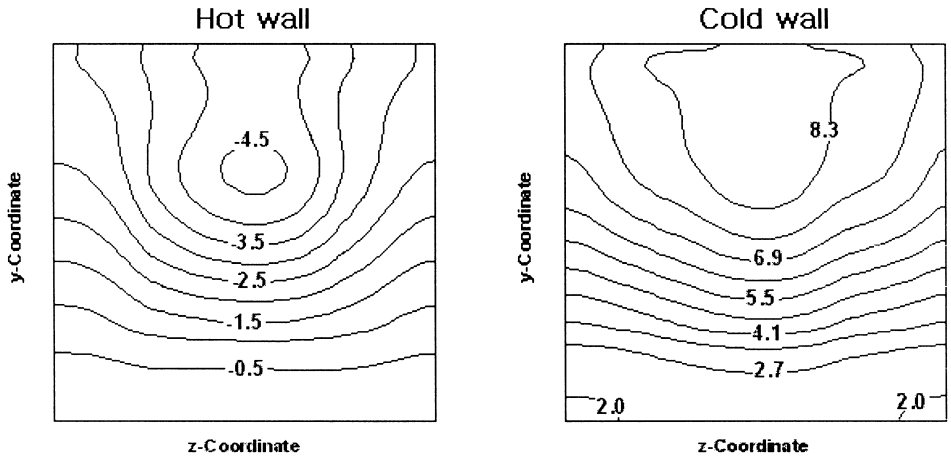

Fig. 19. Local Nusselt number at the hot and cold walls for $Ra = 10^4$ and $\Delta T^* = 25$.

Table 3
Comparison of two- and three-dimensional average Nusselt numbers at the hot and cold walls[a]

		Case 1	Case 2	Case 3	Case 4
$\overline{Nu_h}$	3D	0.691	−3.173	1.170	−2.393
	2D	−0.077	−11.473	0.155	−11.101
$\overline{Nu_c}$	3D	1.487	5.516	1.677	6.023
	2D	2.238	6.759	3.283	7.649

[a] 2D, two-dimensional calculation; 3D, three-dimensional results.

effects due to the temperature difference between the hot and cold walls become larger than those due to the heat transfer from the conducting body to the fluid, resulting in smaller variations in the z-direction than in the case of $\Delta T^* = 2.5$ and $Ra = 10^3$. At $\Delta T^* = 25$, the effects of heat transfer from the conducting body to the fluid are very strong, and the local Nusselt numbers at the hot and cold walls show a large variation in the z-direction for $Ra = 10^3$ and 10^4. The local Nusselt number increases when the Rayleigh number and ΔT^* increase.

4. The presence of a cubic conducting body in a cubic enclosure results in a larger variation of the local Nusselt number at the hot and cold walls in the z-direction, compared to cases without a cubic conducting body in the cubic enclosure, indicating the existence of strong three-dimensionalities of natural convection with a conducting body.

Acknowledgement

This work was supported by the Brain Korea 21 Project.

References

[1] B. Gebhart, Y. Yaluria, R.L. Mahajan, B. Sammakia, Buoyancy-Induced Flows and Transport, Hemisphere, Washington, DC, 1988.
[2] K.T. Yang, Natural convection in enclosures. Handbook of Single Phase Convection Heat Transfer, Wiley, New York, 1987.
[3] S. Ostrach, Natural convection in enclosures, ASME J. Heat Transfer 110 (1988) 1175–1190.
[4] G. de Vahl Davis, I.P. Jones, Natural-convection in a square cavity: a comparison exercise, Int. J. Numer. Methids Fluids 3 (1983) 227–248.
[5] G. de Vahl Davis, Natural convection of air in a square cavity: a benchmark numerical solution, Int. J. Numer. Methods Fluids 3 (1983) 249–264.
[6] G.D. Mallinson, G. de Vahl Davis, Three-dimensional natural convection in a box: a numerical study, J. Fluid Mech. 83 (1977) 1–31.
[7] C.J. Freitas, R.L. Street, A.N. Findikakis, J.R. Koseff, Numerical simulation of three-dimensional flow in a cavity, Int. J. Numer. Meth. Fluids 5 (1985) 561–575.
[8] T. Fusegi, J.M. Hyun, K. Kuwahara, B. Farouk, A numerical study of three-dimensional natural convection in a differentially heated cubical enclosure, Int. J. Heat Mass Transfer 34 (6) (1991) 1543–1557.
[9] R.A.W. Henkes, C.J. Hoogendoorn, Scaling of turbulent natural convection flow in a heated square cavity, ASME J. Heat Transfer 116 (1994) 400–408.
[10] A.M. Lankhorst, C.J. Hoogendoorn, Three-dimensional numerical calculations of high rayleigh number natural convective flows in enclosed cavities, in: Proc. 1988 Natn. Heat Transfer Cong., ASME HTD-96, vol. 3, 1988, pp. 463–470.
[11] S.M. Bilski, J.R. Lloyd, K.T. Yang, An experimental investigation of the laminar natural convection velocity in square and partitioned enclosures, Proc. 8th Int. Heat Transfer Conf. 4 (1986) 1513–1518.
[12] R.J. Krane, J. Jessee, Some detailed field measurements for a natural convection flow in a vertical square enclosure, Proc. 1st ASME-JSME Thermal Engng Joint Conf. 1 (1983) 323–329.
[13] M.S. Bohn, A.T. Kirkpatrick, D.A. Olson, Experimental study of three-dimensional natural convection high-Rayleigh number, J Heat Transfer 106 (1984) 339–345.
[14] J.M. House, C. Beckermann, T.F. Smith, Effect of a centered conducting body on natural convection heat transfer in an enclosure, Numerical Heat Transfer, Part A 18 (1990) 213–225.
[15] J.Y. Oh, M.Y. Ha, K.C. Kim, Numerical study of heat transfer and flow of natural convection in an enclosure with a heat-generating conducting body, Numerical Heat Transfer, Part A 31 (1997) 289–304.
[16] M.Y. Ha, M.J. Jung, Y.S. Kim, A numerical study on transient heat transfer and fluid flow of natural convection in an enclosure with a heat-generating conducting body, Numerical Heat Transfer, Part A 35 (1999) 415–434.